Microchimica Acta (2022) 189: 141
https://doi.org/10.1007/s00604-022-05222-8

ORIGINAL PAPER

Electrochemical sensor based on Ti_3C_2 membrane doped with UIO-66-NH_2 for dopamine

Mingzhen Wen[1] · Ying Xing[1] · Guangyan Liu[1] · Shili Hou[1] · Shifeng Hou[1,2]

Received: 23 October 2021 / Accepted: 7 February 2022 / Published online: 12 March 2022

Abstract

A Ti_3C_2 membrane was prepared by doping UIO-66-NH_2 with Ti_3C_2 through hydrogen bonds. When the doping mass ratio of Ti_3C_2 and UIO-66-NH_2 was 6:1, the electrochemical performance was optimal. Characterization was done by scanning electron microscopy (SEM), transmission electron microscopy (TEM), and electrochemical impedance spectroscopy (EIS) which exhibited hierarchical cave-like physiognomy, large specific area, outstanding electronic conductive network, and excellent film-forming property. Moreover, the Ti_3C_2 film was analyzed via atomic force microscopy (AFM), which displayed good mechanical properties and rough surface morphology. The fabricated Ti_3C_2 membrane/GCE sensor was applied to the detection of dopamine (working potential of + 0.264 V vs. Ag/AgCl) with LOD of 0.81 fM and a sensitivity of 14.72 μA fM^{-1} cm^{-2}. It was demonstrated that the Ti_3C_2 membrane can be used to construct nonenzymatic sensors with excellent performance. The fabricated sensor has high selectivity and stability and has good practicability with recoveries of 101.2–103.5% and a relative standard deviation (RSD) of 1.2–2.4%.

Keywords Ti_3C_2 · UIO-66-NH_2 · Doped membrane · Electrochemical sensors · Differential pulse voltammetry · Dopamine

Introduction

Dopamine (DA) is a crucial catecholamine neurotransmitter of the central nervous system (CNS) [1, 2]. Abnormal dopamine levels can lead to neurological disorders and other diseases, such as schizophrenia, Parkinson's, and Alzheimer's [3–5]. Therefore, the accurate and rapid determination of dopamine is of great significance in developing biomedical science and human health. Due to the simple operation, high sensitivity and selectivity, and immediate response of the electrochemical method, it has attracted considerable attention to detecting dopamine. However, the sensitivity and selectivity of conventional electrodes are not satisfied with the detection of dopamine due to the overlapping in the electrochemical potential window of dopamine with other substances such as uric acid (UA) and ascorbic acid (AA) [6]. Hence, to avoid this disadvantage, novel sensing nanomaterials need to be developed to improve the sensitivity and selectivity of electrochemical sensors.

MXene is a large category of two-dimensional (2D) nanomaterials. It is composed of transition metal carbides and nitrides [7–11]. Recently, MXene-based sensors have been increasingly reported. The functionalized MXene surfaces or combined MXene with other 2D nanomaterials can give the secondary component beneficial properties, resulting in the fabricated MXene-based sensors having more excellent performance than original MXene-based sensors [12–14]. Nevertheless, the conventional challenges for MXene-based sensors are the barrier to commercialization, including realizing significant performance, high stability, versatility, and achieving homogeneous and repeatable amplification processing of MXene-based sensors [12]. Thus, it is vital to improving the properties of composites that the excellent features of MXene construct the required properties of other nanomaterials through self-assembly and additive manufacturing [15].

✉ Shili Hou
houshili@glut.edu.cn

✉ Shifeng Hou
shifenghou@sdu.edu.cn

[1] Guangxi Key Laboratory of Electrochemical and Magnetochemical Functional Materials, College of Chemistry and Bioengineering, Guilin University of Technology, Guilin 541004, People's Republic of China

[2] College of Chemistry and Material Science, Shandong Agricultural University, Taian 271018, People's Republic of China

Metal–organic framework materials (MOF) have become promising nanomaterials in sensing fields due to their high porosity, excellent adsorption performance, film-forming ability, controllable modification synthesis, etc. Therefore, they are considered sensing nanomaterials for fabricating electrochemical sensors [16–18]. However, most MOFs have relatively poor conductivity in aqueous solutions due to the property of coordination bonds. Therefore, because of the excellent features and particular structure of both MXene and MOF, the hybrid materials of MXene combined with MOF can further extend their widespread application in electrochemical sensors.

Herein, a new Ti_3C_2 membrane was prepared from Ti_3C_2 and UIO-66-NH_2 using a hydrogen-bonded self-assembly approach in an aqueous solution with optimal reaction conditions at 60 °C. Ti_3C_2 membrane was realized by the hydrogen bonds between the –OH groups in Ti_3C_2 and the oxygen atoms of O=C groups in UIO-66-NH_2. After the Ti_3C_2 film was freeze-drying, the hierarchical cave-like morphology was found via the scanning electron microscope (SEM). Moreover, the fabricated Ti_3C_2 membrane/GCE was used to detect dopamine via differential pulse voltammetry (DPV). The DPV response for sensing dopamine was obtained through selective oxidation of dopamine forming dopamine quinone in the electrochemical potential window of dopamine, proposed in Fig. 1.

Experimental section

Preparation of Ti_3C_2 membrane

Typically, Ti_3C_2 (0.0343 g) and UIO-66-NH_2 (0.0057 g) were dispersed in ultrapure water (10 mL), and the mixture was magnetically stirred at 60 °C for 6 h. Finally, the obtained sample was freeze-dried.

Fabricating Ti_3C_2 membrane/GCE sensor

Firstly, the bare GCE was polished on the chamois leather with Al_2O_3 (0.05 μm) and repeatedly washed with ultrapure water. Finally, the electrode was dried at room temperature. Then, the solution of the Ti_3C_2 membrane was cast onto the electrode surface. Again, the fabricated electrode was dried at room temperature. Meanwhile, the surface of GCE has formed a uniform film. This film is not fall off or collapse during the test.

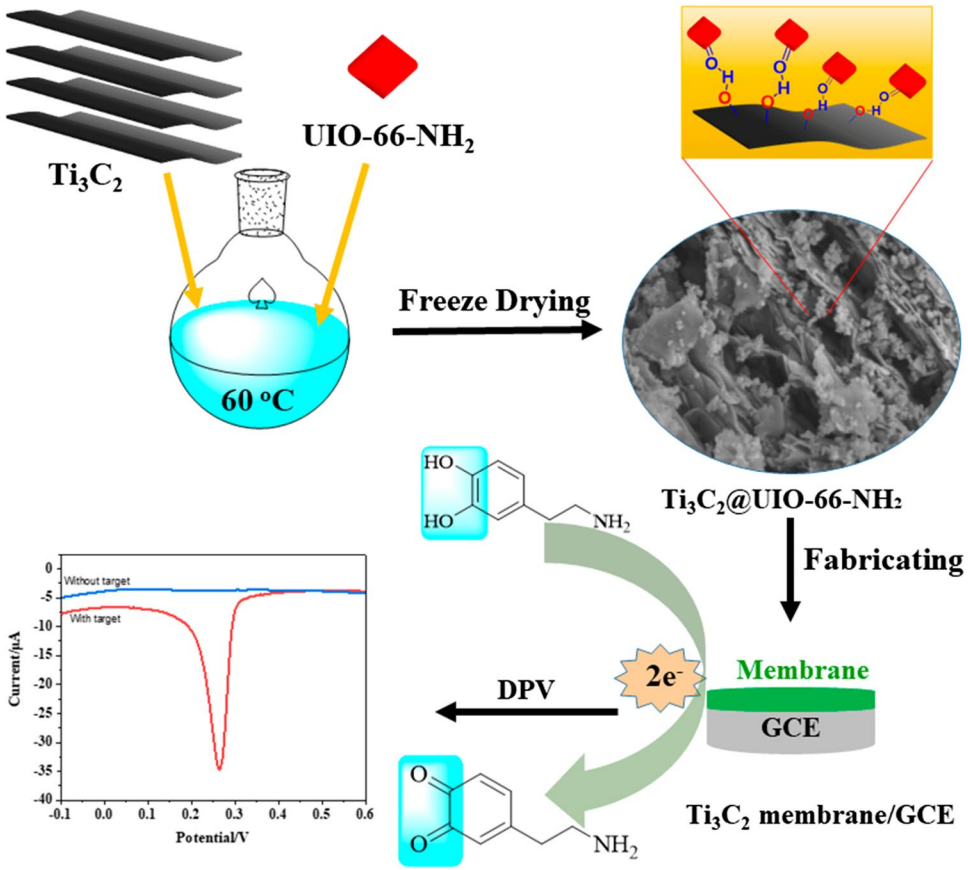

Fig. 1 The synthetic strategy of Ti_3C_2 membrane and the constructed Ti_3C_2 membrane/GCE sensor for sensing dopamine

Results and discussion

Structural characterization

The morphological features of the Ti_3C_2 and Ti_3C_2 membranes were studied via SEM and TEM. As shown in Fig. 2A, Ti_3C_2 exhibits an accordion-like structure with multilayers less than 50 nm. For hierarchical cave-like Ti_3C_2 membrane composite (Fig. 2B), it indicates that UIO-66-NH_2 particles with typical octahedral morphology grow uniformly on the surface of Ti_3C_2. As shown in Fig. 2C, a compact composite Ti_3C_2 film is formed on the electrode surface. Furthermore, as illustrated in Fig. 2D, the diffraction peaks (002) in Ti_3C_2 shift to a smaller angle, agreeing with the reported literature [19]. XRD spectrogram of Ti_3C_2 membrane shows that the typical peak of UIO-66-NH_2 at 6.26° matched well with the peak of Ti_3C_2, revealing that UIO-66-NH_2 particles are successfully grown on Ti_3C_2 nanosheets [20]. Ti_3C_2 nanosheets and UIO-66-NH_2 nanoparticles form a hybrid scaffold as displayed in TEM images of composites at different magnifications (Fig. 2E,F) and energy dispersive X-ray spectrum (EDS) elemental maps (Fig. S2A).

Besides, the Ti_3C_2 membrane on the electrode was characterized using AFM. As shown in Fig. S2B, the Ti_3C_2 film has a flexible nanosheet structure with wrinkles on the surface and offers outstanding transparency. Furthermore, the 3D AFM image of the Ti_3C_2 film provides a more apparent characterization where no cracks, pinholes, or other visible defects, but rather rough surface, demonstrating that the fabricated Ti_3C_2 membrane has outstanding mechanical properties and particular morphology.

In order to further research the mechanism of Ti_3C_2 membrane formation, XPS spectra of the O1s of Ti_3C_2, UIO-66-NH_2, and Ti_3C_2 membrane were recorded. Figure 3A exhibits that the Al element disappears in Ti_3C_2 under the etching action of HF, which makes for its excellent hydrophilicity and dispersion. Moreover, excessive -OH are introduced into Ti_3C_2 during the etching process of Ti_3AlC_2, which will significantly increase the hydrophilicity of Ti_3C_2 and thus form hydrogen bonds. Furthermore, the O1s XPS spectra Ti_3C_2 in Fig. 3B show three peaks at 528.8, 530.0, and 531.6 eV vested in the oxidized TiO_2 phase and the functionalized C−Ti−O_x and C−Ti−O–H phases, respectively [21]. The fourth peak at 532.7 eV is referred to as adsorbed H_2O. For the O1s spectrum of UIO-66-NH_2, the prominent peak, related to the C=O bonds, lies at 531.7 eV, and the second one put down to Zr-O-C locates at lower energy (530.2 eV) [22]. Nevertheless, for Ti_3C_2@UIO-66-NH_2, the O1s spectra exhibit that the main peak appears at lower energy (529.3 eV), indicating the formation of oxygen-containing hydrogen bonds (C-Ti–O•••H•••O=C). Such conversion from Ti_3C_2 to Ti_3C_2@UIO-66-NH_2 can also be reflected in the O1s XPS spectra, where the binding energy of C-Ti–O-H (531.6 eV) is decreased to 529.6 eV

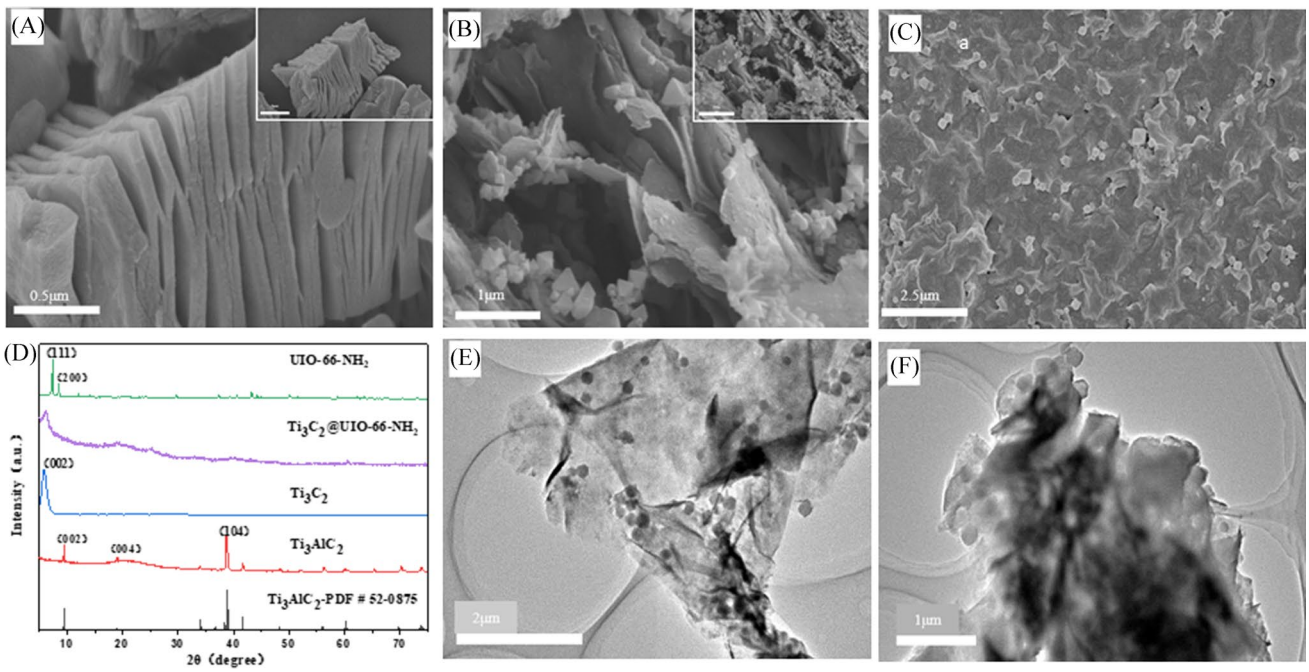

Fig. 2 SEM for Ti_3C_2 (**A**), Ti_3C_2 membrane (**B**), Ti_3C_2 film on electrode (**C**). XRD graph (**D**). TEM for Ti_3C_2 membrane (**E**–**F**). Inset: The magnified SEM images of Ti_3C_2 (**A**), Ti_3C_2 membrane (**B**)

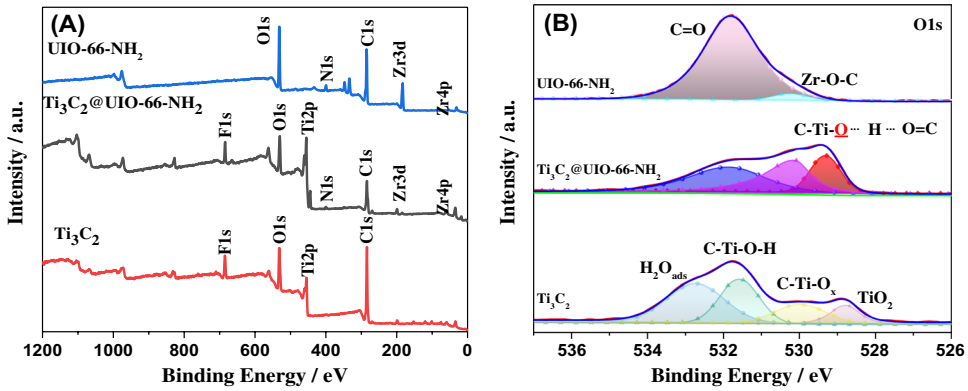

Fig. 3 **A** XPS survey spectra of Ti_3C_2, UIO-66-NH_2, and Ti_3C_2 membrane. **B** The XPS image of O1s regions of Ti_3C_2 membrane

because of the transformation from C-Ti–O-H bonds to C-Ti–O•••H•••O=C bonds.

Electrochemical performance

The CVs for different fabricated electrodes were carried out in $Fe(CN)_6^{3-/4-}$ solution (1 mM) containing KCl (0.1 M) at the potential ranging from − 0.1 V to 0.9 V with a scan rate of 100 mV/s. As can be seen from Fig. 4A, bare GCE and UIO-66-NH_2/GCE exhibit minor symmetrical redox peaks. Nevertheless, the reduction peak current responses of Ti_3C_2 membrane/GCE were significantly increased, indicating that Ti_3C_2 membrane/GCE has sensitive electronic characteristics and strong adsorption capacity. Therefore, it can be suggested that Ti_3C_2 membrane has a better effect on promoting electron transfer, which may root in unique morphology and property of that.

Figure 4B shows the EIS of different modified GCE with 0.19 V open-circuit voltage, 5 mV voltage amplitude, and a frequency ranging from 0.1 to 100 kHz. As can be seen from Fig. 4B, the semicircle diameter of UIO-66-NH_2/GCE (Rct = 133.32 Ω) is much smaller than the case of bare GCE (Rct = 216.00 Ω), indicating that the UIO-66-NH_2 accelerates the electron transport. Whereas Ti_3C_2 membrane/GCE (Rct = 62.53 Ω) has a significantly smaller semicircle diameter than UIO-66-NH_2/GCE (Rct = 133.32 Ω), indicating that the electron transfer on the surface of the electrode was accelerated through Ti_3C_2 membrane, that is to say, Ti_3C_2 outstanding enhances the electrical conductivity. The results are consistent with CV results.

Sensor capability of the Ti_3C_2 membrane/GCE

The Ti_3C_2 membrane/GCE sensor capability for detecting DA was studied via DPV method under the optimum experimental conditions (See Supporting Information), at the potential ranging from − 0.1 to 0.6 V with 100 mV s^{-1} scan rate. As can be seen from Fig. 5A,B, the DPV response

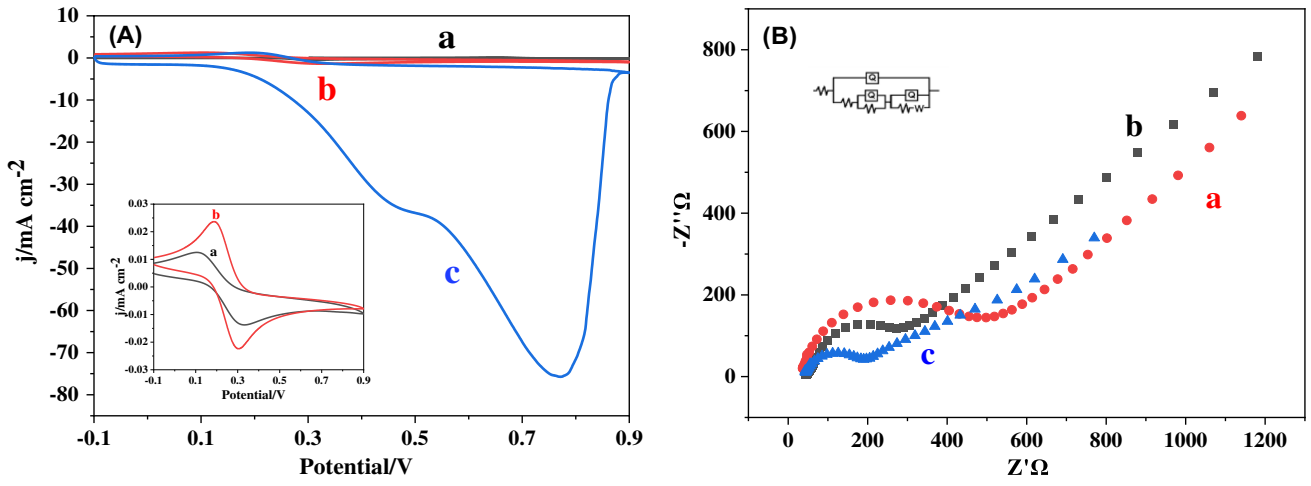

Fig. 4 **A** CVs of bare GCE (a), UIO-66-NH_2/GCE (b), and Ti_3C_2 membrane/GCE (c) in $Fe(CN)_6^{3-/4-}$ solution of 1 mM including KCl of 0.1 M. Scan rate: 100 mV s^{-1}. Inset: Amplified CV plot of bare GCE (a) and UIO-66-NH_2/GCE (b). **B** Nyquist diagrams of bare GCE (a), UIO-66-NH_2/GCE (b), and Ti_3C_2 membrane/GCE (c) in $Fe(CN)_6^{3-/4-}$ solution of 1 mM including 0.1 M KCl

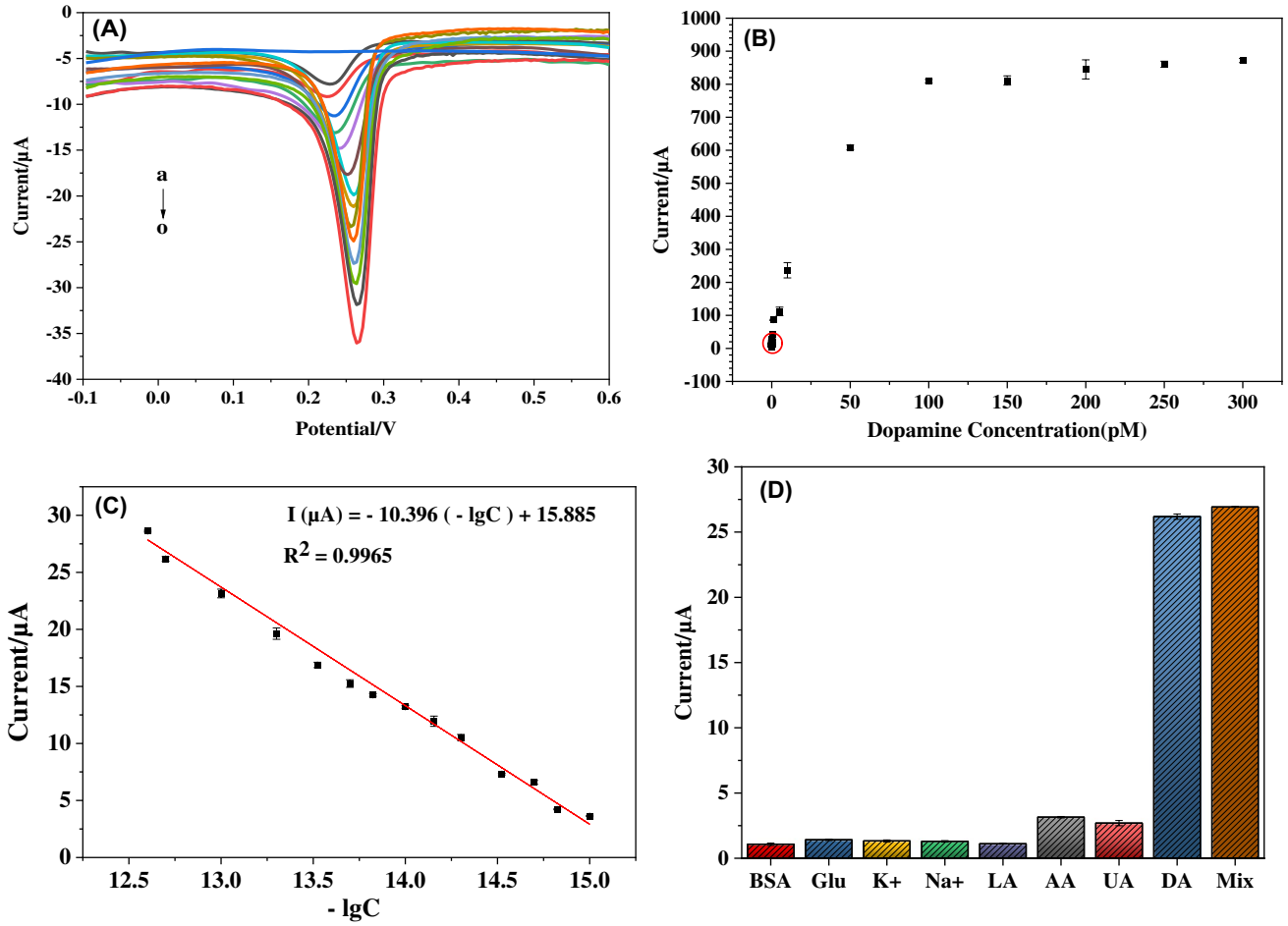

Fig. 5 **A** DPV of Ti_3C_2 membrane/GCE sensor with different concentrations of DA (a ~ o: 0, 1, 1.5, 2, 3, 5, 7, 10, 15, 20, 30, 50, 100, 200, 250 fM, respectively) in PBS (1 mM, pH 7.0). **B** Analyzed the DA detection range of the fabricated sensor. **C** Calibration chart for DA concentrations from 1 to 250 fM. **D** The interference of various species for DA detection

of the fabricated sensor was significantly enhanced as the concentration of DA increased from 0 to 100 pM. However, when DA concentration reached 100 pM and above, the DPV response of the fabricated sensor was gradually stabilized, indicating that the conductance of the fabricated sensor was gradually saturated [23]. Furthermore, as shown in Fig. 5C, the DPV responses heightened with increasing DA concentration, demonstrating an excellent linear dependence between the current (I) and negative logarithm of DA concentration (−lgC) ranging from 1 to 250 fM with 14.72 μA fM^{-1} cm^{-2} sensitivity. The linear regression equation was I (μA) = − 10.396 (−lgC) + 15.885 (R^2 = 0.9965). The limit of detection (LOD) was 0.81 fM. The sensing performances of the sensor and the reported electrochemical sensors for identifying DA are shown in Table 1. Moreover, the reported other methods for detecting DA are listed in Table S1. As can be seen from Table 1 and S1, the performance of the Ti_3C_2 membrane/GCE sensor was superior to the reported electrochemical sensors and even suitable for placement among the reported other methods for the sensing DA with a long linear range and low LOD. The remarkable capability of the sensor was ascribed to the synergistic outcomes of the unique morphology and good conductivity of the Ti_3C_2 membrane.

Interference, reproducibility, and stability studies

Because the oxidative potential of DA overlaps with the signals of AA and UA, it is easy to affect the detection of DA on the electrode. Therefore, the selectivity for the constructed sensor was determined with potential interfering substances containing K^+, Na^+, Glu, LA, BSA, AA, and UA. As shown in Fig. 5D, tested substances do not interfere obviously with 200 fM DA. Thus, this sensor has an outstanding anti-interference capability for detecting DA.

Besides, the Ti_3C_2 membrane/GCE sensor's long-term stability was investigated by examining its DPV response after storage at 4 °C. As shown in Fig. S8, after 15 days, the

Table 1 The reported electrochemical sensors for detecting DA

Sensing electrode	Methods	LOD (μM)	Linear Range (μM)	Sensitivity ($\mu A \cdot \mu M^{-1}$)	Interference studies	Reference
RGO/GCE	DPV	0.074	0.20–13.0	-	-	[24]
NCZ-MMO/GCE	DPV	0.00001	0.001–500	2.31	UA, AA, Glu, BSA, EPI	[25]
$Ni(OH)_2$NCs@MnO_2 NSs CSA/GCE	[a]I-t	0.00175	0.02–16.3 18.3–118.6	0.033 0.088	Glu	[26]
PPy/ZIF-67-MIPs/Nafion/GCE	I-t	0.0308	0.08–100 100–500	0.052 0.0259	K^+, Na^+, Co^{2+}, Ca^{2+}, Mg^{2+}	[27]
PVIM/Co_5POM@CNT/[b]GE	DPV	0.0005	0.0005–600	-	AA	[28]
C-h-BN/GCE	CV	0.0058	0.01–40.0 40–300	0.379 0.18	UA, AA	[29]
PA/GO/GCE	DPV	0.016	0.05–10	4.56	UA, AA	[30]
Graphene Ink electrode	DPV	0.001	0.000005–0.5	-	UA, AA	[31]
PPy/Fe_3O_4/RGO/GCE	DPV	0.00233	0.007–1.2	-	UA, AA	[32]
ZnO/Carbon paste	[c]SWV	0.056	0.3–100	-	AA, Glu, CA, MT, EA etc	[33]
NiFeP/GCE	SWV	0.0003	0.01–500	-	UA, AA, Glu	[34]
MXene/DNA/Pd/Pt/GCE	DPV	0.03	0.2–1000	-	UA, AA, Glu	[35]
MXene/ZnS/GCE	DPV	1.39	90–820	12.1	CA, AA, Glu	[36]
Ti_3C_2@UIO-66-NH_2/GCE	DPV	0.81(fM)	1–250(fM)	14.72 $\mu A\ fM^{-1}cm^{-2}$	BSA, AA, UA, LA, Glu, K^+, Na^+	This work

[a]Chronoamperometry; [b]Graphite electrode; [c]Square Wave Voltammetry

sensor maintains more than 92.1% of its initial response to DA, resulting in excellent standing stability, and the reproducibility of this sensor was further evaluated via detecting 200 fM DA under the same conditions (Fig. S9). Five independent sensors yielded 3.16% relative standard deviation (RSD) under the same method, demonstrating excellent reproducibility.

Real sample detection

To appraise the application of the Ti_3C_2 membrane/GCE sensor in practice, which was used to detect spiked DA from human serum samples [37–39]. Drug-free human blood samples were collected from healthy volunteers at the Guilin University of Technology Hospital. All the blood samples were obtained through venipuncture, and the coagulant was added rapidly. Due to the high protein of DA bonding in the blood plasma, these serum samples were pretreated using a high-speed refrigerated centrifuge to eliminate the interferences and improve the recovery [40–43]. Then, 100 μL of blood serum was diluted with 5 mL of 0.1 M PBS (pH = 7.0) buffer to prevent the matrix effect of actual samples [44]. Different concentrations of DA standard solution were selected according to the linear range and added to the diluted serum samples to prepare the spiked samples. Then, the determination of dopamine was carried out through DPV with the applied potential (+0.264 V vs. Ag/AgCl). Finally, the recovery rates were calculated according to reference [45]. As shown in Table 2, the results indicated that the recoveries were 101.2% to 103.5%, with the RSD in the range of 1.2–2.4%. The obtained result shows that the Ti_3C_2 membrane/GCE sensor has remarkable recoveries of DA on biological samples.

Table 2 Results for the detection of dopamine in human serum samples ($n = 5$)

Samples	DA in diluted sample (fM)	Added (fM)	Found (fM)	RSD (%)	Recovery (%)
Sample I	0	50.0	50.9	1.3	101.5
	0	100.0	102.6	2.2	102.7
	0	200.0	200.7	1.2	101.2
Sample II	0	50.0	51.2	1.5	101.8
	0	100.0	102.9	2.4	103.5
	0	200.0	202.7	2.3	103.1

Conclusion

A novel Ti_3C_2 membrane has been synthesized from hydrogen-bonded self-assembly in a water solution with a large specific area, distinguishing electronic conductivity network, and excellent dispersion in the aqueous phase. These outstanding performances played a significant role in electron transfer and fabricating sensors. Astonishingly, the fabricated sensor of the Ti_3C_2 membrane exhibited a substantial performance for DA with high selectivity and sensitivity. Moreover, the fabricated sensor was further applied to fast-sensing DA in the real samples with excellent recoveries. This study indicates that the applications of some novel prepared MXene membranes in sensor fields are still in the initial stage, meaning that the fabricated hybrid materials of MXene combined with properties of other materials will have promising application prospects. Nowadays, the COVID-19 pandemic spreads around the world; more advanced sensors are urgently needed with high sensitivity and selectivity, rapid determination, and commercialization. This work opens a direction to building advanced sensors using MXene-based nanomaterials.

Supplementary Information The online version contains supplementary material available at https://doi.org/10.1007/s00604-022-05222-8.

Funding This work was supported by Guangxi Science and Technology Department (No. 2018AD19154 and 2021AC20002), Foundation of Guilin University of Technology, Guangxi Key Laboratory of Electrochemical and Magneto-chemical Functional Materials, and College Students' Innovative Entrepreneurial Training Plan Program (No. 202010596028 and No. 202110596531).

Declarations

Conflict of interest The authors declare no competing interests.

References

1. Sajid M, Nazal MK, Mansha M, Alsharaa A, Jillani SMS, Basheer C (2016) Chemically modified electrodes for electrochemical detection of dopamine in the presence of uric acid and ascorbic acid: a review. TrAC Trends Anal Chem 76:15–29. https://doi.org/10.1016/j.trac.2015.09.006
2. Ferapontova EE (2017) Electrochemical analysis of dopamine: perspectives of specific in vivo detection. Electrochim Acta 245:664–671. https://doi.org/10.1016/j.electacta.2017.05.183
3. Azadbakht A, Roushani M, Abbasi AR, Menati S, Derikvand Z (2016) A label-free aptasensor based on polyethyleneimine wrapped carbon nanotubes in situ formed gold nanoparticles as signal probe for highly sensitive detection of dopamine. Mater Sci Eng C 68:585–593. https://doi.org/10.1016/j.msec.2016.05.077
4. Salamon J, Sathishkumar Y, Ramachandran K, Lee YS, Yoo DJ, Kim AR, Gnanakumar G, (2015) One-pot synthesis of magnetite nanorods/graphene composites and its catalytic activity toward electrochemical detection of dopamine. Biosens Bioelectron 6:269–276. https://doi.org/10.1016/j.bios.2014.08.085
5. Li BR, Hsieh YJ, Chen YX, Chung YT, Pan CY, Chen YT (2013) An ultrasensitive nanowire-transistor sensor for detecting dopamine release from living PC12 cells under hypoxic stimulation. J Am Chem Soc 135:16034–16037. https://doi.org/10.1021/ja408485m
6. Wang J, Zeng Y, Wan L, Zhao J, Yang J, Hu J, Miao F, Zhan W, Chen R, Liang F (2020) Catalyst-free fabrication of one-dimensional N-doped carbon coated TiO_2 nanotube arrays by template carbonization of polydopamine for high performance electrochemical sensors. Appl Surf Sci 509:145301. https://doi.org/10.1016/j.apsusc.2020.145301
7. Naguib M, Kurtoglu M, Presser V, Lu J, Niu J, Heon M, Hultman L, Gogotsi Y, Barsoum MW (2011) Two-dimensional nanocrystals produced by exfoliation of Ti_3AlC_2. Adv Mater 23:4248. https://doi.org/10.1002/adma.201190147
8. Naguib M, Mashtalir O, Carle J, Presser V, Lu J, Hultman L, Gogotsi Y, Barsoum MW (2012) Two-dimensional transition metal carbides. ACS Nano 6:1322–1331. https://doi.org/10.1021/nn204153h
9. Mashtalir O, Naguib M, Mochalin VN, Dall'Agnese Y, Heon M, Barsoum MW, Gogotsi Y (2013) Intercalation and delamination of layered carbides and carbonitrides. Nat Commun 4:1716. https://doi.org/10.1038/ncomms2664
10. Lukatskaya MR, Mashtalir O, Ren CE, Dall'Agnese Y, Rozier P, Taberna PL, Naguib M, Simon P, Barsoum MW, Gogotsi Y (2013) Cation intercalation and high volumetric capacitance of two-dimensional titanium carbide. Science 341:1502–1505. https://doi.org/10.1126/science.1241488
11. Khazaei M, Arai M, Sasaki T, Chung CY, Venkataramanan NS, Estili M, Sakka Y, Kawazoe Y (2013) Novel electronic and magnetic properties of two-dimensional transition metal carbides and nitrides. Adv Funct Mater 23:2185–2192. https://doi.org/10.1002/adfm.201202502
12. Ho DH, Choi YY, Jo SB, Myoung JM, Cho JH (2021) Sensing with MXenes: progress and prospects. Adv Mater 2005846.https://doi.org/10.1002/adma.202005846
13. Yoon J, Shin M, Lim J, Lee JY, Choi JW (2020) Recent advances in MXene nanocomposite-based sensors. Sensors 10:185. https://doi.org/10.3390/bios10110185
14. Shi X, Wang H, Xie X, Xue Q, Zhang J, Kang S, Wang C, Liang J, Chen Y (2019) Bioinspired ultrasensitive and stretchable MXene-based strain sensor via nacre-mimetic microscale "brick-and-mortar" architecture. ACS Nano 13:649–659. https://doi.org/10.1021/acsnano.8b07805
15. VahidMohammadi A, Rosen J, Gogotsi Y (2021) The world of two-dimensional carbides and nitrides (MXenes). Science 372:abf1581. https://doi.org/10.1126/science.abf1581
16. Hu Z, Deibert BJ, Li J (2014) Luminescent metal-organic frameworks for chemical sensing and explosive detection. Chem Soc Rev 43:5815–5840. https://doi.org/10.1039/c4cs00010b
17. Cui L, Wu J, Li J, Ju H (2015) Electrochemical sensor for lead cation sensitized with a DNA functionalized porphyrinic metal–organic framework. Anal Chem 87:10635–10641. https://doi.org/10.1021/acs.analchem.5b03287
18. Wang Y, Hou C, Zhang Y, He F, Liu M, Li X (2016) Preparation of graphene nanosheet bonded PDA/MOF microcapsules with immobilized glucose oxidase as a mimetic multi-enzyme system for electrochemical sensing of glucose. J Mat Chem B 4:3695–3702. https://doi.org/10.1039/c6tb00276e
19. Xu H, Yin X, Li X, Li M, Liang S, Zhang L (2019) Lightweight Ti_2CT_x MXene/Poly(vinyl alcohol) composite foams for electromagnetic wave shielding with absorption-dominated feature. ACS Appl Mater Interfaces 11:10198–10207. https://doi.org/10.1021/acsami.8b21671

20. Gu Y, Wu YN, Li L, Chen W, Li F, Kitagawa S (2017) Controllable modular growth of hierarchical MOF-on-MOF architectures. Angew Chem Int Ed 56:15658–15662. https://doi.org/10.1002/anie.201709738
21. Wang X, Shen X, Gao Y, Wang Z, Yu R, Chen L (2015) Atomic-scale recognition of surface structure and intercalation mechanism of Ti_3C_2X. J Am Chem Soc 137:2715–2721. https://doi.org/10.1021/ja512820k
22. Jayaramulu K, Horn M, Schneemann A, Saini H, Bakandritsos A, Ranc V, Petr M, Stavila V, Narayana C, Scheibe B, Štěpán Kment, Otyepka M, Motta N, Dubal D, Zbořil R, Fischer RA (2021) Asymmetric supercapacitors: Covalent Graphene-MOF hybrids for high-performance asymmetric supercapacitors (Adv. Mater. 4/2021). Adv Mater 33:2170028. https://doi.org/10.1002/adma.202170028
23. Xu B, Zhu M, Zhang W, Zhen X, Pei Z, Xue Q, Zhi C, Shi P (2016) Ultrathin MXene-micropattern-based field-effect transistor for probing neural activity. Adv Mater 28:3333–3339. https://doi.org/10.1002/adma.201504657
24. Yin B, Zhai HL, Zhao BQ, Bi KX, Mi JY (2021) Chemometric-sassisted simultaneous voltammetric determination of multiple neurotransmitters in human serum. Bioelectrochemistry 139:107739. https://doi.org/10.1016/j.bioelechem.2021.107739
25. Durai L, Gopalakrishnan A, Badhulika S (2021) One-pot hydrothermal synthesis of NiCoZn a ternary mixed metal oxide nanorod based electrochemical sensor for trace level recognition of dopamine in biofluids. Mater Lett 298:130044. https://doi.org/10.1016/j.matlet.2021.130044
26. Yang T, Tian L, Zhou E, He G, Chen D, Xie J (2019) Design of $Ni(OH)_2$ nanocages@MnO_2 nanosheets core-shell architecture to jointly facilitate electrocatalytic dynamic for highly sensitive detection of dopamine. Biosens Bioelectron 143:111634. https://doi.org/10.1016/j.bios.2019.111634
27. Zhang W, Duan D, Liu S, Zhang Y, Leng L, Li X, Chen N, Zhang Y (2018) Metal-organic framework-based molecularly imprinted polymer as a high sensitive and selective hybrid for the determination of dopamine in injections and human serum samples. Biosens Bioelectron 118:129–136. https://doi.org/10.1016/j.bios.2018.07.047
28. Thakur N, Das Adhikary S, Kumar M, Mehta D, Padhan AK, Mandal D, Nagaiah TC (2018) Ultrasensitive and highly selective electrochemical detection of dopamine using poly (ionic liquids)-cobalt polyoxometalate/CNT composite. ACS Omega 3:2966–2973. https://doi.org/10.1021/acsomega.7b02049
29. Ouyang H, Li W, Long Y (2021) Carbon-doped h-BN for the enhanced electrochemical determination of dopamine. Electrochim Acta 369:137682. https://doi.org/10.1016/j.electacta.2020.137682
30. Wang D, Xu F, Hu J, Lin M (2017) Phytic acid/graphene oxide nanocomposites modified electrode for electrochemical sensing of dopamine. Mater Sci Eng C 71:1086–1089. https://doi.org/10.1016/j.msec.2016.11.023
31. Butler D, Moore D, Glavin NR, Robinson JA, Ebrahimi A (2021) Facile post-deposition annealing of graphene ink enables ultrasensitive electrochemical detection of dopamine. ACS Appl Mater Interfaces 13:11185–11194. https://doi.org/10.1021/acsami.0c21302
32. Wang Y, Zhang Y, Hou C, Liu M (2016) Ultrasensitive electrochemical sensing of dopamine using reduced graphene oxide sheets decorated with p-toluenesulfonate-doped polypyrrole/Fe_3O_4 nanospheres. Microchim Acta 183:1145–1152. https://doi.org/10.1007/s00604-016-1742-6
33. Molaakbari E, Mostafavi A, Beitollahi H (2015) Simultaneous electrochemical determination of dopamine, melatonin, methionine and caffeine. Sens Actuator B 208:195–203. https://doi.org/10.1016/j.snb.2014.10.130
34 Thakur N, Chaturvedi A, Mandal D, Nagaiah TC (2020) Ultrasensitive and highly selective detection of dopamine by a NiFeP based flexible electrochemical sensor. Chem Commun 56:8448–8451. https://doi.org/10.1039/D0CC03583A
35. Zheng JS, Wang B, Ding AL, Weng B, Chen JC (2018) Synthesis of MXene/DNA/Pd/Pt nanocomposite for sensitive detection of dopamine. J Electroanal Chem 816:189–194. https://doi.org/10.1016/j.jelechem.2018.03.056
36. Arif N, Gul S, Sohail M, Rizwan S, Iqbal M (2021) Synthesis and characterization of layered Nb_2C MXene/ZnS nanocomposites for highly selective electrochemical sensing of dopamine. Ceram Int 47:2388–2396. https://doi.org/10.1016/j.ceramint.2020.09.081
37. Khan AF, Brownson DAC, Randviir EP, Smith GC, Banks CE (2016) 2D hexagonal boron nitride (2D-hBN) Explored for the Electrochemical Sensing of Dopamine. Anal Chem 88:9729–9737. https://doi.org/10.1021/acs.analchem.6b02638
38. Sivasubramanian R, Biji P (2016) Preparation of copper (I) oxide nanohexagon decorated reduced graphene oxide nanocomposite and its application in electrochemical sensing of dopamine. Mater Sci Eng B 210:10–18. https://doi.org/10.1016/j.mseb.2016.04.018
39. Zhang W, Liu L, Li Y, Wang D, Ma H, Ren H, Shi Y, Han Y, Ye BC (2018) Electrochemical sensing platform based on the biomass-derived microporous carbons for simultaneous determination of ascorbic acid, dopamine, and uric acid. Biosens Bioelectron 121:96–103. https://doi.org/10.1016/j.bios.2018.08.043
40. Tahmasebi E, Yamini Y, Saleh AE (2009) Extraction of trace amounts of pioglitazone as an anti-diabetic drug with hollow fiber liquid phase microextraction and determination by high-performance liquid chromatography-ultraviolet detection in biological fluids. J Chromatogr B 877:1923–1929. https://doi.org/10.1016/j.jchromb.2009.05.033
41. Mojtaba S, Maryam S, Khosro K, Nasrin M, Sayyed HK (2012) A novel quantum dot-laccase hybrid nanobiosensor for low level determination of dopamine. Analyst 137:5553–5559. https://doi.org/10.1039/C2AN36035G
42. Huang H, Gao Y, Shi FP, Wang GN, Shah SM, Su XG (2012) Determination of catecholamine in human serum by a fluorescent quenching method based on a water-soluble fluorescent conjugated polymer–enzyme hybrid system. Analyst 137:1481. https://doi.org/10.1039/C2AN16143E
43. Wang Y, Xiao Y (2012) Glassy carbon electrode modified with poly (dibromofluorescein) for the selective determination of dopamine and uric acid in the presence of ascorbic acid. Microchim Acta 178:123–130. https://doi.org/10.1007/s00604-012-0821-6
44. Nada FA, Maher FE (2010) Novel poly(3-methylthiophene)/Pd, Pt nanoparticle sensor: synthesis, characterization and its application to the simultaneous analysis of dopamine and ascorbic acid in biological fluids. Sens Actuators B Chem 145:299–310. https://doi.org/10.1016/j.snb.2009.12.014
45. Ma JP, Bai WS, Liu XL, Zheng JB (2022) Electrochemical dopamine sensor based on bi-metallic Co/Zn porphyrin metal–organic framework. Microchim Acta 189:20. https://doi.org/10.1007/s00604-021-05122-3